PROCEEDINGS, 46th Workshop on Geothermal Reservoir Engineering
Stanford University, Stanford, California, February 15-17, 2021
SGP-TR-218

Constant Flow Rate Fracturing with Different Fracturing Fluids for Enhanced Geothermal Systems

Guoqing Jian[1], Ramesh S. Sarathi[1], Carlos A. Fernandez[1*], Jeff Burghardt[1], Alain Bonneville[1], Varun Gupta[1] and Geoffrey Garrison[2]

1. Pacific Northwest National Laboratory, Richland, WA, United States

2. Altarock Energy, Inc. Seattle, WA, United States

carlos.fernandez@pnnl.gov

Keywords: StimuFrac, polyallylamine (PAA), CO_2-reactive polymer, fracturing, STOMP

ABSTRACT

Objectives/Scope: StimuFrac, a CO_2-reactive polymer aqueous solution [polyallylamine (PAA) 1wt% in water], can be used as a less water-intensive fracturing fluid for enhanced geothermal systems (EGS) based on laboratory-scale investigations. Fracturing tests from inch scale samples indicate that StimuFrac in the presence of CO_2 could generate fractures with high conductivity at lower breakdown pressures compared with water, CO_2, and a combination of water/CO_2 fracturing processes. The objective of this work is to study the performance of patented StimuFrac fluid in ½ foot side rock samples under representative EGS pressure/temperature conditions and reveal the mechanisms governing the fracturing process assisted with multiphase flow numerical simulations using Subsurface Transport Over Multiple Phases (STOMP).

Methods/Procedures/Process: StimuFrac was evaluated using a high-temperature true-triaxial fracturing apparatus and ½ foot side granite cubic samples. Three representative fracturing fluids including water, CO_2, CO_2 with water were used as control. The fluid transport was simulated with STOMP based on a home-built model which is designed with feedback from the experimental setup and conditions.

Results/Observations/Conclusions: For all the water "only" fracturing tests, the conductivity of the rock fractured is quite low (less than 2 μm^3 based on radial flow assumption). All three CO_2-based fracturing fluids, i.e., CO_2 injected in hot dry rock (HDR), CO_2 injected in rock partially saturated with water, and CO_2 injected in rock partially saturated with aqueous PAA (1wt%), fractured granite at higher breakdown pressures, high transient flow rates, and generated higher-conductivity fractures as compared to water. In addition, faster pressurization rates with CO_2-based fracturing fluids are found to be associated with higher fracture conductivities. When partially saturating the rock sample with 1wt% PAA aqueous solution followed by fracturing with CO_2, the volume expansion and viscosity increase triggered by CO_2-induced cross-linking of PAA leads to a faster pressure increase than CO_2/water and dry CO_2. This faster pressurization rate is possibly caused by (1) decrease in relative permeability of CO_2 compared to that for the uncrosslinked CO_2/water system, and (2) a decreased leakoff due to the increase in viscosity of PAA. It was also found that CO_2 as a fracturing fluid injected in HDR can generate high fracture conductivity only when injected at very high flow rates (10 mL/min). However, the conductivity of CO_2 fracturing in HDR is highly variable while CO_2 injected in rock partially saturated PAA consistently generates large fractures with significantly lower variability in conductivity values. In addition, CO_2/PAA fracturing fluid system generates fractures with the highest conductivity independently of injection flow rates and using 1/6 of the mass of CO_2 as compared to CO_2 injected in HDR. The fractured rock samples show that all three CO_2-based fracturing fluids, CO_2 injected in HDR, CO_2 injected in rock partially saturated with water, and CO_2 injected in rock partially saturated with aqueous PAA, can generate larger fracture planes than water. From the simulation pressure distribution map of water fracturing, we observed a plateau (water vapor pressure) of the pressure distribution of water in the radial direction of rock which hinders the fracture propagation. STOMP modeling results show a higher pressurization length for PAA/CO_2 than other fluids, which may contribute to the consistently higher conductive fractures generated.

Applications/Significance/Novelty: The results of this study suggest CO_2/PAA as the best performing stimulation fluid under the studied geothermal P/T conditions. CO_2/PAA offers the following three additional advantages over waterless CO_2, and CO_2/water fracturing fluids: 1) it requires significantly lower volumes of CO_2 due to the reduced leak off, 2) large fractures can be generated reproducibly and independently of CO_2 injection flow rate, and 3) the reversible viscosity (Shao et al. 2015) increase is beneficial to transport proppants when they become available for enhanced geothermal systems.

1. INTRODUCTION

Enhanced geothermal systems (EGS) are designed to extract energy from geothermal reservoirs containing hot rock but insufficient natural permeability or fluid saturation. In an EGS, cold, high-pressure fluid is injected into the reservoir under carefully controlled conditions. The pressurized fluid opens pre-existing fractures and flows through them, gradually increasing in temperature as it travels towards a production well. EGS(Lund and Freeston 2001; Lund, Freeston, and Boyd 2005; Lund 2011; Lund and Boyd 2016) are considered as an attractive alternative to fossil energy because geothermal energy is renewable and its extraction generates low CO_2 emissions.

Hydraulic fracturing is recognized as an efficient way to further increase the permeability of the hot rock, and, as a result, the injectivity and heat exchange efficiency. To fracture the hot rock, operators need advanced stimulation fluids and tools that can withstand the high-

temperature environments, but many current technologies are designed for low temperatures (e.g., below 120 °C) applications. For example, gellants such as xanthan gum used to increase viscosity and enable proppant transport in tight oil and gas recovery cannot withstand temperatures above 120 °C. It is crucial to develop fracturing fluids that can efficiently fracture hot reservoirs without undergoing degradation of their chemical components. As importantly, operators need stimulation technologies that reduce water requirements, as EGS fracturing operations require on average ten times the water (Chabora et al. 2012; Bradford et al. 2014) needed for tight oil stimulation operations. Therefore, research efforts have been also directed to develop alternative fluids that either reduce or completely replace water without a negative impact on fracturing performance.

In this regard, waterless fluid technologies (Isaka et al. 2019; Song et al. 2019), including propellants and fluids such as CO_2, and N_2, have been explored at small scales and in shallow reservoirs. The high-pressure pulses generated by propellants can initiate fractures though concerns remain about their ability to propagate fractures beyond the near-wellbore region and their safe deployment. Our group has recently developed CO_2-reactive fracturing fluids that undergo a volume expansion triggered by the crosslinking reactions between an aqueous polymer solution (polyallylamine (PAA)) and CO_2. These reactions and the resulting volume expansion are favored at high temperatures. We demonstrated that this fracturing fluid, hereafter called StimuFrac^{TM} or simply PAA, can mediate a reversible chemically-activated expansion and viscosity increase in confined environments (B. Jung et al. 2015; Shao et al. 2015; Fernandez et al. 2019). Indeed, high pressure/temperature laboratory-scale experiments that simulated geothermal reservoir conditions at different depths (different confining P and T) demonstrated efficient fracture creation on Coso reservoir samples and in non-porous fused silica samples with rock-like mechanical properties (Fernandez et al. 2019).

Nevertheless, questions remain regarding how the CO_2-triggered volume expansion and rheo-reversible properties impact fracturing performance and how to deploy and optimize StimuFrac-based stimulations. In this work, we report on a series of fracturing experiments in larger (1/2-foot side) cubic granite rocks and compare the performance of the StimuFrac (PAA aqueous solution)/CO_2 stimulation fluid to that of water, CO_2, and water/CO_2 in terms of breakdown pressure, permeability enhancement, and volumes of fluid used.

2. MATERIALS AND METHODS

2.1 Fracturing procedure

A borehole is drilled longitudinally through each sample and the sample is placed in the fracturing apparatus as described in our previous studies(Jian et al. 2020). The loading frame creates the principal stress that directs the fracture orientation as occurs in the field. The stress field used in this test is $\sigma_{T-B}/\sigma_{N-S}/\sigma_{W-E}$ =7.58/9.65/9.65 MPa (1100/1400/1400 psi) which means the stress in the direction perpendicular to the top and bottom of the rock sample is the minimum principal stress, and its value equals 7.58 MPa (1100 psi). The other two stresses are perpendicular to the south and north faces and to the east and west faces, respectively, and are equal to 9.65 MPa (1400psi). All experiments were performed under identical temperature conditions. Four different stimulation tests were performed on half-foot cubic rock samples (Sierra White granite), as shown in Fig. 1, at constant flow rate mode. A notch in the horizontal (radial) direction was created (about 0.1mm deep) and the wellbore was polished to facilitate the introduction of the casing without damaging the O-rings that provide zonal isolation.

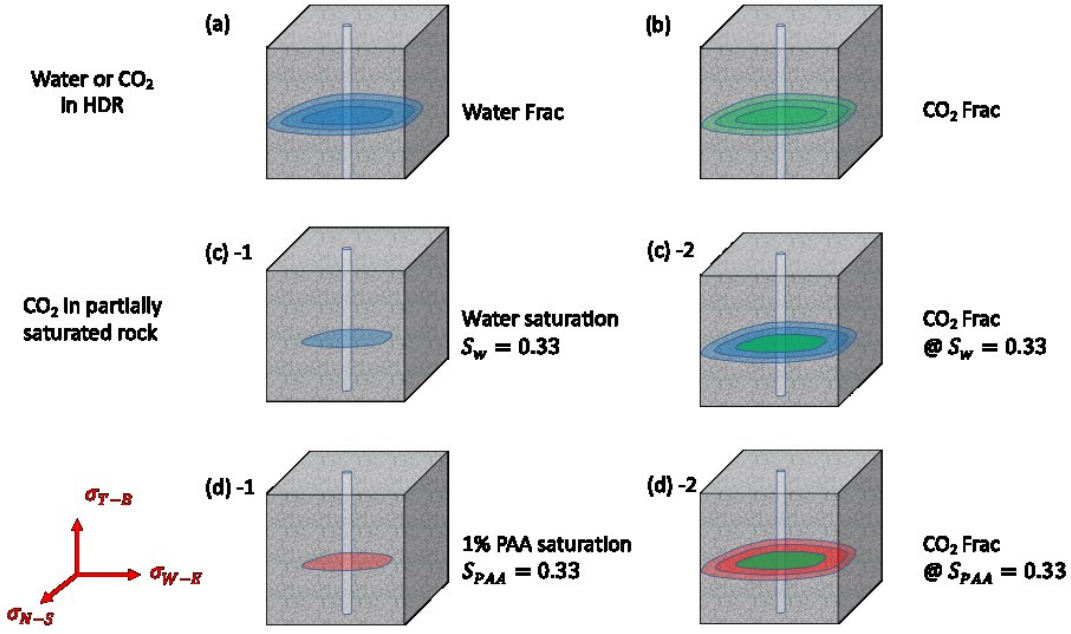

Fig. 1. Four injection strategies for hydraulic fracturing including (a) water fracturing in hot dry rock (HDR); (b) CO_2 fracturing in HDR; (c) CO_2 fracturing with rock pre-saturated with water S_w=0.33; (d) CO_2 fracturing with rock pre-saturated with aqueous S_{PAA}=0.33; Rock dimension=6"×6"×6"

Four stimulation strategies or stimulation fluids were used, each of which differ in the initial fluid saturation conditions they create in the sample, and/or in which fluid is used to drive the fracture. For each of the four strategies, the fracture can be driven using either a constant-rate injection or using a series of constant-pressure steps. The four stimulation strategies are described next.

For the first stimulation strategy, referred to in Fig. 1(a), water was first injected in constant-pressure mode at 6.89MPa (1000 psi) which is higher than saturated water vapor pressure 1.55 MPa (225 psi) at 200 °C. After the flow rate due to leakoff reached a nominally steady state, the water fracturing was initiated with constant flow rate mode until the rock fracture is estimated to have been driven to the edge of the sample. In the plots shown later in the paper, this stimulation strategy is labeled simply H_2O.

For the second strategy, referred to in Fig. 1 (b), CO_2 is first injected in constant-pressure mode at 8.96 MPa (1300 psi) until CO_2 reach the wellbore. After that, the CO_2 fracturing is initiated with constant flow rate mode until the fracture is estimated to have been driven to the edge of the sample. In the plots shown later in the paper this strategy is labeled simply CO_2.

For the third strategy, CO_2 injection in water partially saturated porous matrix referred to in Fig. 1 (c), water is injected into the wellbore in constant-pressure mode at 8.27 or 8.96 MPa (1200/1300 psi) until a pre-defined volume of water has been injected. The volume of fluid was chosen to be equal to 1/3 of the estimated pore volume. The porosity was estimated to be 1%. This should result in an initial aqueous phase saturation equal to approximately 0.33. What should be noted that the saturation distribution of the water could be heterogeneous such as a higher liquid saturation is near the wellbore and a lower water saturation is away from wellbore. This distribution is highly dependent on the capillary number of the fluid system in the rock pores. The whole stimulation process and corresponding saturation are as follow. In the beginning, the rock is dry which means it is undersaturated for water phase (wetting phase) and nearly 100% saturated with air, with an expected trace amount of water trapped in the sub-nano pores (vapor pressure significantly lower than that for a flat water/gas interface at 200ºC). This phenomenon is called capillary condensation and can be described by the Kelvin equation. Once the bulk water phase reaches the wellbore, the spontaneous imbibition occurs due to capillary pressure suction. Once the saturation is above the connate water saturation, an external pressure gradient from the rock center to the surface is needed to increase the water saturation. On one hand, the superficial velocity of the water phase at any point of the rock along the route from the wellbore to the surface decreases slightly due to radial flow. The viscosity of the water phase is assumed to be constant (~0.13 mPa×s) at 200°C within a large pressure range above the vapor pressure. The interfacial tension between gas/liquid increases from the wellbore to the rock surface due to pressure decrease. Thus, the capillary number, which is the product of viscosity and superficial velocity divided by the interfacial tension, can change at different locations in the rock and will ultimately determine the saturation of the water phase. On the other hand, during this gas desaturation process (liquid displaces gas), if the capillary number is high enough, a high liquid saturation (>0.33 which is the average value) can occur near the wellbore. This will inevitably lead to saturation decline from the wellbore to the surface of the rock. After this water pre-saturation period, CO_2 is injected in constant-pressure mode at 8.27 or 8.96 MPa (1200 psi or 1300psi). After the flow rate reached a nominal steady-state due to leakoff (about 300 seconds), additional CO_2 is added to the sample in constant flow-rate mode. In the plots shown later this strategy is referred to as CO_2/H_2O.

The fourth strategy, CO_2 injection in porous matrix partially saturated with an aqueous solution of PAA referred to in Fig. 1 (d), is identical to the CO_2/H_2O strategy except that instead of pre-saturating the rock sample with water, a 1 wt% PAA aqueous solution was used. In the plots shown later in the paper this strategy is referred to as CO_2/PAA.

2.2 Preparation of rock thin sections and optical microscopy analysis

The thin section was prepared from the split rock surfaces. Different minerals were stained with different colors. The color codes by stains of thin section are: K-Feldspar Stain(yellow); Plagioclase Stain (orange red); Calcite Stain (pink red); Iron Stain(blue); Others(quartz): white or grey or else. Red fluorescent epoxy was used for vacuum/pressure impregnation. A microscope (type 020-520.716 DM LM/P, Bartels & Stout, Inc. distributed by Leica) was used and a camera (Model#LU1276C-CLX, Clemex Technologies Inc) was connected to the microscope to capture the images of thin sections with 100× or 50× magnifications.

3. RESULTS AND DISCUSSIONS

3.1 Stimulation with water

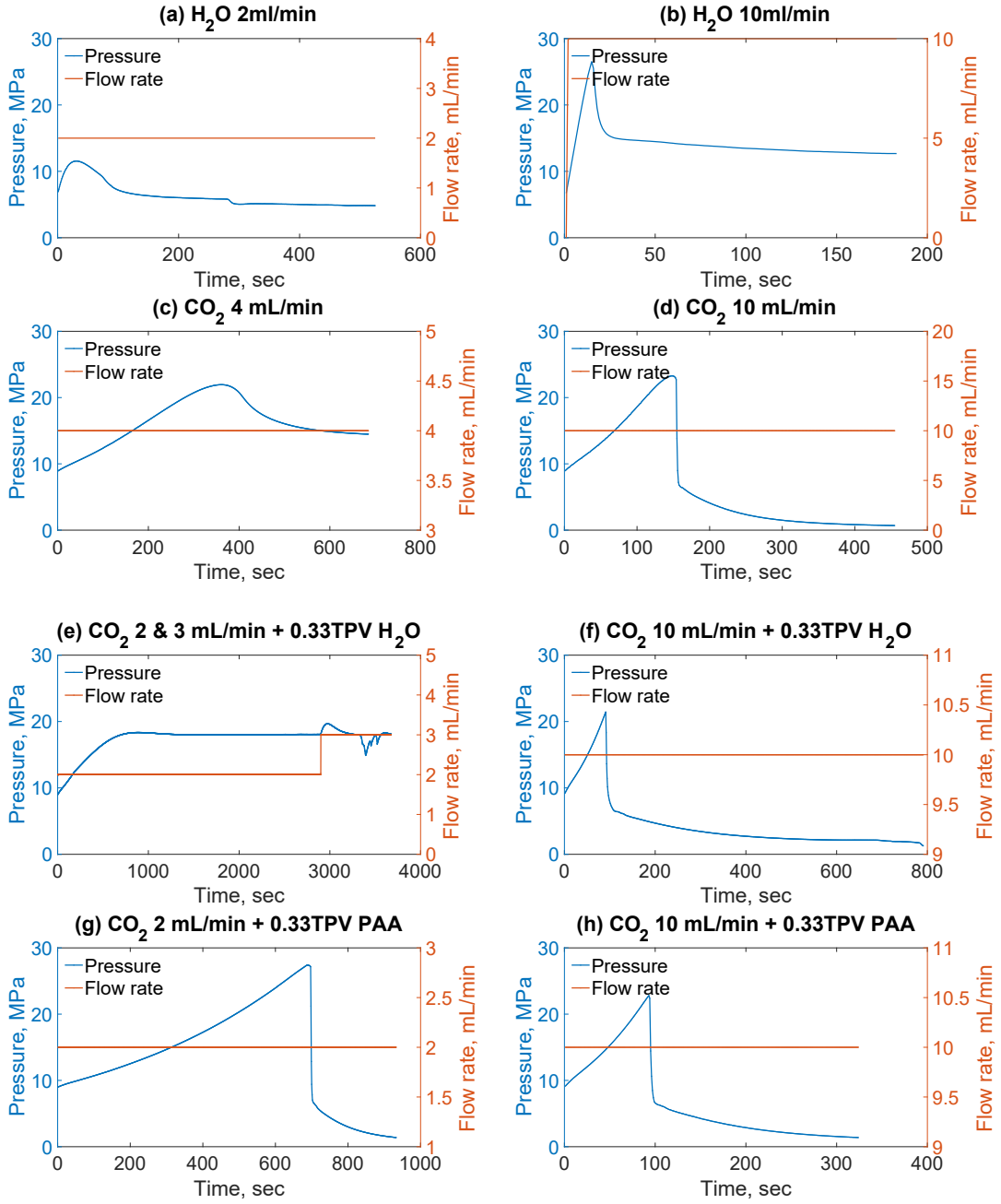

Fig. 2. Water fracturing at (a) constant flow mode (2 mL/min) in rock B3, (b) constant flow mode (10 mL/min) in rock B4; CO_2 fracturing at (c) constant flow mode (4 mL/min) in rock B10, (d) constant flow mode (10 mL/min) in rock B2; CO_2/H_2O fracturing at (e) constant flow mode (2~3 mL/min) in rock B1, (f) constant flow mode (10 mL/min) in rock B1 , CO_2/PAA fracturing at (g) constant flow mode (2 mL/min) in rock A10, (h) constant flow mode (10 mL/min) in rock D7.

For fracturing using constant flow rate as shown in Fig. 2(a) and Fig. 2(b), water was pressurized to 6.89 MPa (1000psi) first, then the pump was changed to constant flow rate mode (2 mL/min or 10 mL/min or 25 mL/min) and water was injected into the wellbore until the rock fractured.

3.2 Stimulation with CO_2

Fig. 2(c) to (d) shows the pressure history plots for fracturing tests performed injecting CO_2 in HDR. The CO_2 fracturing was conducted at constant flow mode (4 mL/min) (c), constant flow mode (10 mL/min) (d). CO_2 was pressurized to 8.27/8.96MPa (1200/1300psi) within

the pump before injection. For fracturing using constant flow rate as shown in Fig. 2(c) and Fig. 2(d), CO_2 was pressurized to 8.96MPa (1300psi) first, then the pump was switched to constant flow rate (4 mL/min or 10 mL/min) and CO_2 was injected into the wellbore until the rock fractured.

3.3 Stimulation with CO_2/H_2O

Fig. 2(e) to (f) show pressure history plots for one of the fracturing tests performed injecting water at constant pressure to saturate about 1/3 of the total pore volume (TPV) followed by injection of CO_2 in constant flow mode. For fracturing using constant flow rate [Fig. 2(e) and Fig. 2(f)], CO_2 was pressurized to 8.96MPa (1300psi) first with the pump in constant pressure mode. Then, the pump was switched to constant flow mode (2 & 3 mL/min or 10 mL/min) and CO_2 was injected into the wellbore. For the experiments where CO_2 is injected at (constant flow rate) 2 mL/min [Fig. 2(e)], the pressure stabilizes and reaches a steady state. Therefore, the flow rate was increased to 3 mL/min with a resulting temporary increase in pressure followed by a pressure reduction to steady values similar to the ones observed at 2 mL/min. No rock breakdown was observed. The pressure fluctuation observed during the injection of CO_2 at 3 mL/min in rock partially saturated with water may be caused by the water saturation changes due to drainage at a high fractional flow of the wetting phase(water).

3.4 Stimulation with CO_2/PAA

Similar to the above-described injection of CO_2 in granite partially saturated with water (1/3 of TPV), CO_2 was injected in granite with 1/3 of the TPV saturated with a 1 wt% aqueous solution of PAA. For fracturing experiments injecting CO_2 at constant flow rate [Fig. 2(g) and Fig. 2(h)], CO_2 was first pressurized to 8.27/8.96MPa (1200/1300psi). Then the pump was switched to constant flow rate mode (2 mL/min or 10 mL/min) and CO_2 was injected into the wellbore followed by penetrating the rock partially saturated with the 1 wt% aqueous solution of PAA. Contrary to the case where the rock was partially saturated with pure water [Fig. 2(e)], CO_2 fractured the rock partially saturated with PAA when the flow rate was 2 mL/min.

3.5 Diagram of conductivity and breakdown pressure (Pb)/pressurization rate

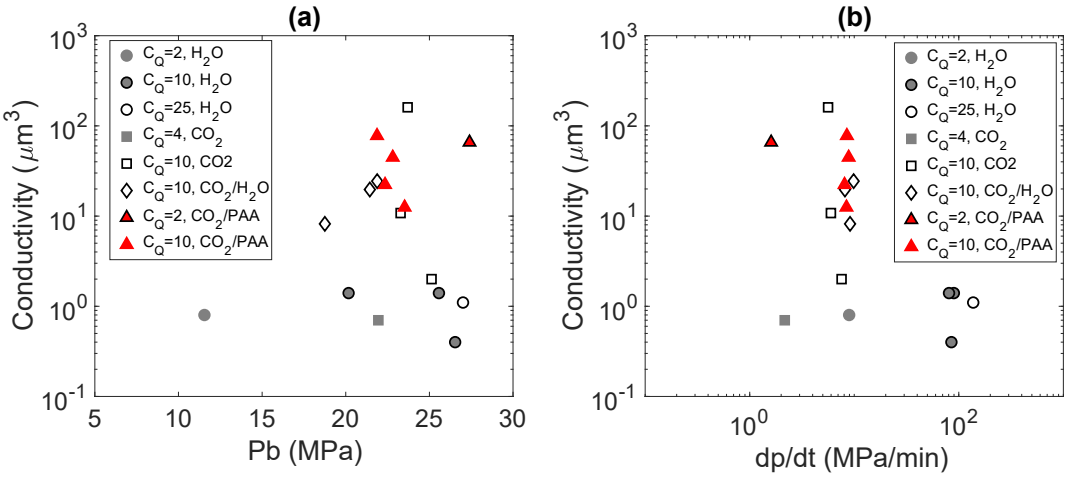

Fig. 3. Diagram of conductivity and breakdown pressure of fracturing results; (a) conductivity versus breakdown pressure with different injection modes; (b) conductivity of fracture generated as a function of pressurization rate of fluids injected.

Table 1 and Fig. 3 illustrate a summary of the fracturing tests performed at constant flow rate. Table 1 reports values of breakdown pressure, fracture conductivity, permeability and aperture, as well as water (or aqueous PAA), and CO_2 mass consumption. The injected masses of water (or 1% PAA) and CO_2 were calculated within the time range between the beginning of constant flow rate injection to the time when breakdown pressure was reached. For water, since the density change is negligible, the mass-consumed can be calculated by the product of volume consumed and the density. In the case of CO_2, the density changes significantly with temperature and pressure changes during the fracturing process. Therefore, for constant flow rate injection, Table 1 reports a range of CO_2 mass delivered, the lower value is estimated assuming an isothermal process within the pump (the value could be negative which means the assumption of isothermal is wrong, thus this lower boundary of mass consumption will need to be set to be 0 to make it physically meaningful) and the upper value can be estimated by Equation of State for gases assuming an adiabatic process.

The diagram of conductivity versus breakdown pressure for the different fracturing fluids is shown in Fig. 3. All the tests were conducted at 200 ºC. The circle symbols in Fig. 3 represent the first stimulation strategy, water injection in HDR. The breakdown pressure ranged from 9.65 MPa (1400 psi) to 11.72 MPa (1700 psi), with fracture conductivity values lower than 2 mm^3 independently of injection strategy. Furthermore, the fracture hydraulic conductivity was still below 2 mm^3 even when the injection flow rate was as high as 25 mL/min with an associated breakdown pressure of 26.89 MPa (3900 psi). The second stimulation strategy, i.e., CO_2 injection in HDR (square symbols in Fig. 3) generated fractures with a wide range of conductivity values. When injecting CO_2 in HDR using constant flow rate mode the conductivity is also low for 4 mL/min but noticeably increases (2.0~4.2 mm^3, 10.8~23.1 mm^3, and 160~341 mm^3) at high (10 mL/min) flow rates though with fracture conductivity values that differ by an order of magnitude. Diamond symbols in Fig. 3 represent CO_2/H_2O stimulation strategy, fracturing efficiency was negligible at low injection rates and only good at high injection rates (10 mL/min) with

conductivity values in the 8.2~51.9 mm^3 range. The fourth stimulation strategy, CO_2/PAA (triangles symbols in Fig. 3), CO_2/PAA consistently attained very large conductivity values (with two of the largest measured) independently of injection flow rate (10 mL/min: 12.5~139.5 mm^3; 2 mL/min: 65.7~139.5 mm^3). It is also important to note that CO_2/PAA stimulation strategy consistently generated highly conductive fractures independently of injection mode.

Table 1 Summary of fracturing results with different fluids with constant flow rate injection mode

Test	Rock ID	Mode/Rate	Strategy	P_b	C_f	K_f	h	m_{H_2O} / m_{PAA}	m_{CO_2}
		(mL/min)		(MPa)	(μm^3)	(μm^2)	(μm)	(g)	(g)
1	B3	$C_Q = 2$	H_2O	11.55	0.8~1.7	0.4~0.6	2.1~2.7	0.9	0
2	D4	$C_Q = 10$	H_2O	26.54	0.4~0.8	0.2~0.4	1.7~2.1	1.3	0
3	D5	$C_Q = 10$	H_2O	25.57	1.4~2.9	0.5~0.9	2.5~3.3	0.8	0
4	D6	$C_Q = 10$	H_2O	20.17	1.4~3.0	0.6~0.9	2.6~3.3	1.2	0
5	B8	$C_Q = 25$	H_2O	27.01	1.0~2.1	0.4~0.7	2.3~2.9	0.6	0
6	B10	$C_Q = 4$	CO_2	21.95	0.7~1.5	0.4~0.6	2.0~2.6	0	9.7~14.5
7	B2	$C_Q = 10$	CO_2	23.70	160.6~341.1	12.9~21.3	12.4~16.0	0	7.8~12.8
8	C1	$C_Q = 10$	CO_2	23.28	10.8~23.1	2.2~3.6	5.0~6.5	0	4.0~8.3
9	C7	$C_Q = 10$	CO_2	25.13	2.0～4.2	0.7~1.1	2.9~3.7	0	5.6~9.5
10	B1	$C_Q = 2\ or\ 3$	CO_2/H_2O	N/A	No frac	No frac	No frac	11.3	N/A
11	B1	$C_Q = 10$	CO_2/H_2O	21.44	19.7~41.8	3.2~5.3	6.2~7.9	11.3	0~2.5
12	C8	$C_Q = 10$	CO_2/H_2O	21.88	24.4~51.9	0.7~1.1	6.6~8.5	11.3	0~2.1
13	C9	$C_Q = 10$	CO_2/H_2O	18.75	8.2~17.5	1.8~3.0	2.9~3.7	11.3	0~1.9
14	A10	$C_Q = 2$	CO_2/PAA	27.40	65.7~139.5	7.1~11.8	9.2~11.9	11.3	1.1~4.9
15	B7	$C_Q = 10$	CO_2/PAA	22.81	44.7~95.0	5.5~9.1	8.1~10.5	11.3	0~2.3
16	D3	$C_Q = 10$	CO_2/PAA	21.87	77.7~165.1	8.0~13.2	9.8~12.6	11.3	0~0.9
17	D7	$C_Q = 10$	CO_2/PAA	22.35	22.3~47.3	3.5~5.7	6.4~8.3	11.3	0~0.9
18	D8	$C_Q = 10$	CO_2/PAA	23.52	12.5~26.5	2.4~3.9	5.3~6.8	11.3	0~2.0

As shown in Table 1, for the CO_2/H_2O stimulation strategy (entry 10), when the flow rate of injected CO_2 equals to 2mL/min or 3 mL/min, the rock does not fracture because the leak-off from the wellbore exceeds this flow rate and pressure doesn't build up. Similarly, when injecting CO_2 in HDR at low/intermediate flow rates the stimulation generate low fracture conductivity (entry 6).

As shown in Fig. 3(a), high conductivity values of fracture are obtained when the breakdown pressure is high. This is likely due to the high transient flow rate to the fracture following breakdown, which is enhanced by the higher compressibility of CO_2 compared to water. As stated earlier, the CO_2/PAA stimulation strategy resulted in slightly higher conductivity than the CO_2/H_2O strategy for the constant flow rate mode.

Fig. 3(b) shows the effect of the pressurization rate of fracturing fluids on the fracture conductivity. Pressurization rate is calculated based on the fluid pressure increase divided by the time when rock fractures. In general, for all stimulation strategies, the higher the pressurization rate, the higher is the fracture conductivity. The exception is all the tests conducted with the H_2O injected in HDR strategy, where the conductivity of fracture generated is less than 2 mm^3 even at flow rates as high as 25 mL/min. For the second stimulation strategy, CO_2 injected in HDR, low injection rates generate low conductivity fractures while rapid (constant flow, 10 mL/min) injection generates conductivity values with large variability (up to two orders of magnitude). The same applies to stimulation strategy CO_2/H_2O, i.e., CO_2

injected in rock partially saturated with water. As shown in Fig. 3(b), when the pressurization rate is around 5~10 MPa/min, the conductivity of the fracture is large but when the pressurization rate is low, the conductivity of the fracture is low or no fracture occurs (see also entry 10). The exception is the injection strategy corresponding to CO_2 is injected in rock partially saturated with PAA aqueous solution (CO_2/PAA). This stimulation strategy consistently generated highly conductive fractures independently of pressurization rate as can be seen in entry 14 to 18 of Table 1. The reason for this will be discussed next.

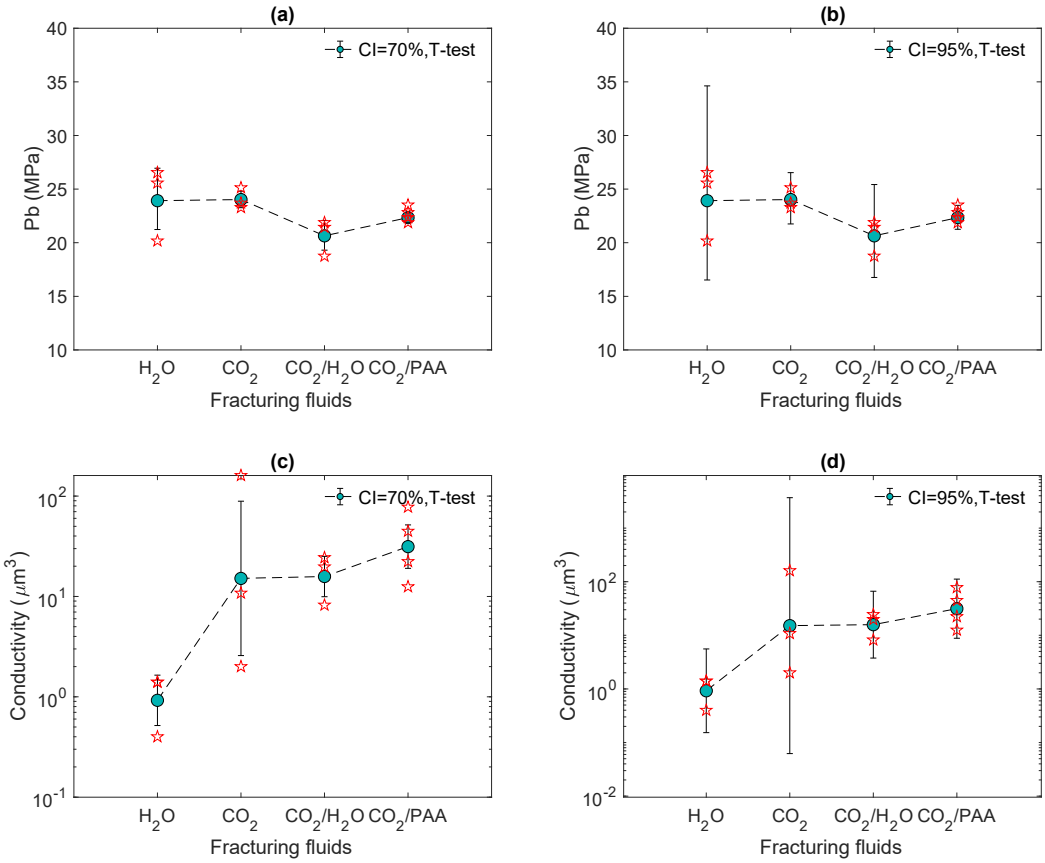

Fig. 4 Diagram of breakdown pressure of fracturing results with all four fracturing strategies at 10 mL/min; (a) breakdown pressure for different fracturing fluids with 70% confidence interval; (b) breakdown pressure for different fracturing fluids with 95% confidence interval; (c) conductivity for different fracturing fluids with 70% confidence interval; (d) conductivity for different fracturing fluids with 95% confidence interval.

Fig. 4(a) and (b) are plots of the observed mean breakdown pressures (marker) with student's t-distribution assuming a lognormal distribution. A lognormal distribution(Heath 1967) is used because it is generally more appropriate for strength/fracture estimations since it only admits positive values. To estimate confidence intervals for a lognormal underlying distribution, the standard student t-analysis is performed on the logarithm of the data, which follows a normal distribution if the data itself follows a lognormal distribution. Then, once confidence intervals have been defined for the logarithm of the data, they can be exponentiated to convert them back to the standard data space. This same approach is taken for the fracture conductivity (plots c and d). The error bars indicate the 70% confidence interval for the true mean. At this level of confidence at 10 mL/min injection rate, the CO_2/PAA has a higher true mean breakdown pressure than CO_2/H_2O and lower than CO_2 in HDR. Water has a higher degree of variability at 10 mL/min than the CO_2-based fluids. This does not make it possible to say anything about the breakdown pressure difference between CO_2-based fluids and water at this injection rate.

Fig. 4(c) and (d) are plots of the observed mean fracture conductivity values for each testing condition along with confidence intervals using the same approach discussed above, assuming that the fracture conductivity will follow a lognormal distribution(Bee, Massart, and Neveu 1995). The bottom left plot (c) has error bars drawn at the 70% confidence level, and the bottom right (d) plot shows error bars for the 95% confidence level.

At 10 mL/min there is greater than a 70% confidence that all CO_2-based fluids outperform water and greater than 70% confidence that CO_2/PAA performs better than CO_2/H_2O. Based on the data we cannot say that the CO_2/PAA and CO_2/H_2O produce any difference compared to the CO_2 HDR case. That is because of a single CO_2 test that had a conductivity of 160.6 μm^3 compared to the others that were 10.8 μm^3 and 2.0 μm^3, giving the CO_2 data a very high degree of uncertainty. We can also say with greater than 95% confidence that the performance of CO_2/PAA is greater than water at 10 mL/min. As shown in Table 2, for the breakdown pressure t-test, there is no

difference of mean values using different fracturing fluids (p< a=0.05, 95% confidence level). When a =0.3 (70% confidence level), it can be concluded that for the mean values of breakdown pressure: $P_b(CO_2/H_2O) < P_b(CO_2/PAA) < P_b(H_2O)$ and $P_b(CO_2/H_2O) < P_b(CO_2/PAA) < P_b(CO_2)$. There is no statistical difference (70% or 95% confidence level) in breakdown pressure using H_2O or CO_2 when injecting at 10 mL/min. For the t-test regarding conductivity, when a =0.3, it can be concluded that the mean values of fracture conductivity $C_f(H_2O) < C_f(CO_2/H_2O) < C_f(CO_2/PAA)$. There is no statistical difference for C_f at 70% confidence level using CO_2 and CO_2/H_2O or CO_2 and CO_2/PAA.

Table 2 t-Test for constant flow rate fracturing (10 mL/min)

	Breakdown pressure (P_b), t-test					Conductivity (C_f), t-test			
p value	H_2O	CO_2	CO_2/H_2O	CO_2/PAA	p value	H_2O	CO_2	CO_2/H_2O	CO_2/PAA
H_2O	×	0.965	0.228	0.587	H_2O	×	0.150	0.007	0.002
CO_2	0.965	×	0.070	0.103	CO_2	0.150	×	0.977	0.633
CO_2/H_2O	0.228	0.070	×	0.190	CO_2/H_2O	0.007	0.977	×	0.244
CO_2/PAA	0.587	0.103	0.190	×	CO_2/PAA	0.002	0.633	0.244	×

3.6 Wellbore pressure and flow history of fracturing fluids deployed in constant flow rate injection mode

Fig. 5 shows wellbore pressure history with all four stimulation strategies/fluids performed in constant flow rate mode. Fig. 5 shows that when injecting water in HDR fractures are generated at significantly higher breakdown pressure at higher flow rates (10mL/min and 25 mL/min). However, the transient flow rate (Fig. 6 discussed in the next section) is low and the fractures generated have very low conductivity fractures. Fig. 5 (b) also shows results with the second stimulation strategy, CO_2 injected in HDR. Fracturing test performed at 4mL/min shows that the rock is fractured with a slow fracture propagation process (dark blue plot), at a relatively low breakdown pressure, and attaining a fracture with the lowest conductivity (0.7~1.5 μm^3). However, when the flow rate of CO_2 in HDR is increased to 10mL/min, the rock is fractured significantly faster (red, orange, and purple plots in Fig. 5 (b)) and attaining fractures with higher (though markedly variable) conductivity values. Three fracturing tests at 10 ml/min constant flow rate were performed injecting CO_2 in HDR as stimulation strategy. For the first of these tests (red plot), the breakdown pressure was 23.27 MPa (3375 psi) while for the second test (yellow plot) it was 23.28 MPa (3376psi), and for the third test (magenta plot) the breakdown pressure was 25.13MPa (3645psi). However, once the fracture initiates, the first two tests show a different CO_2 transport behavior in the rock with fracture propagation. From the pressure response plots, the first two curves (red and yellow plots) deviate from each other once the pressure of the wellbore is around 6.21 MPa (900 psi) and this pressure value is just below the minimum principal stress of 7.58 MPa (1100 psi). This suggests that above this point, i.e., when the fracture is created, there is a positive net pressure and the two fractures have similar hydraulic properties. However, once the fractures are closed (at a negative net pressure or pressure below the minimum principal stress), the two fractures behave differently. The first stimulation test with CO_2 in HDR (red plot) shows a considerably sharper pressure decline curve below 6.21 MPa (900 psi) which indicates a significantly larger fracture compared to the fracture obtained in the second stimulation test given the fact that the flow rates of CO_2 at the pump are identical in both tests (10 mL/min). The conductivity measured for the largest fracture is around 160.6~341.1 μm^3 (red plot, first stimulation test with CO_2 in HDR at 10 mL/min) while for the second test performed under identical conditions the fracture conductivity is around 10.8~23.1 μm^3. For the third CO_2 fracturing in HDR, a much smoother pressure decline curve was observed and the fracturing conductivity was only 2.0~4.2 μm^3. The reason why these three-fracturing tests show similar breakdown pressure, but very different conductivity is still unclear. One of the possible hypotheses could be associated with differences in rock heterogeneity or even minute natural fractures that could exist in the rock matrix systems which would affect the fracture initiation and propagation process.

Fig. 5 (c) and (d) show results for CO_2/H_2O and CO_2/PAA stimulation strategies/fluids, respectively under high and low flow rate conditions. A comparison of stimulation at low flow rate is shown in Fig. 5 (e). These tests were carried out with a CO_2 flow rate of 2 mL/min in rock partially saturated with water or 1wt% aqueous PAA (1/3 of TPV). For the fracturing test with CO_2/H_2O stimulation fluid, the sample does not fracture the rock due to the leak-off rate accommodating the entire injected flow rate of CO_2. The pressure reaches a plateau at a constant flow rate of 2 mL/min. However, for a fracturing test performed with CO_2/PAA stimulation fluid, the pressure curve separates from that of the CO_2/H_2O stimulation test at approximately 250 seconds and at a pressure of approximately 15.17 MPa (2200 psi) as shown in Fig. 5 (e). The curve separation could be caused by 1) in-situ crosslinking reaction between CO_2 and PAA resulting viscosity increase, 2) volume expansion induced saturation-increase of aqueous phase. For the CO_2/H_2O two-phase saturated system, the relative permeability of the gas phase(Jian et al. 2019) based on Corey's model is expressed as shown in Eq. (1), thus the increased water saturation could cause a reduction of relative permeability for the supercritical CO_2 phase. Therefore, when the superficial velocity of the supercritical CO_2 phase is constant, the pressure gradient will increase according to Darcy's law as shown in Eq. (2).

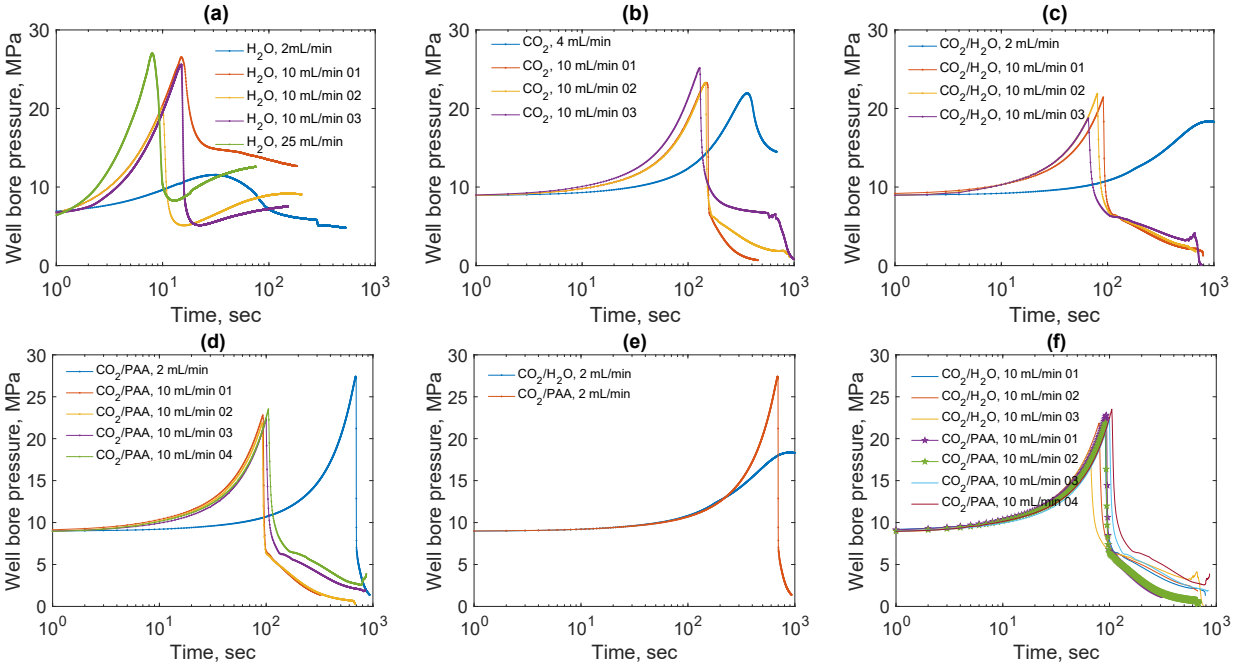

Fig. 5. Wellbore pressure history plots of all four stimulation strategies in constant flow rate mode (a) H_2O in HDR, Q=2 or 10 mL/min; (b) CO_2 in HDR, Q=4 or 10 mL/min; (c) CO_2/H_2O, Q=2 or 10 mL/min; (d) CO_2/PAA, Q=2 or10 mL/min. (e) CO_2/H_2O and CO_2/PAA, Q=2 mL/min; (f) CO_2/H_2O and CO_2/PAA, Q=10 mL/min. All stimulation tests were conducted at 200°C.

$$k_{rg} = k_{rg}^{0} * \left(\frac{1-S_w-S_{wc}}{1-S_{grw}-S_{wc}}\right)^{n_g} \quad (1)$$

Where k_{rg}^{0} is the endpoint relative permeability of gas; S_w is the water saturation; S_g is the gas saturation; S_{wc} is the connate water saturation; S_{grw} is the residual gas saturation to water; n_g is the exponent coefficient of gas in Corey's relative permeability model.

$$\mu_g = -\frac{k_{rock} * k_{rg}}{u_g} * \nabla P \quad (2)$$

Where μ_g is the viscosity of the gas phase; k_{rock} is the permeability of rock; k_{rg} is the relative permeability of gas; ∇P is the pressure gradient across the rock; u_g is the superficial velocity.

For high flow rate stimulation tests, CO_2/H_2O (10 mL/min) and CO_2/PAA (10 mL/min), the results show that when injecting CO_2 in the presence of PAA, two of the pressure decline curves (green and purple line with star marker) after fracturing occurs are sharper than any of the curves obtained when injecting CO_2 in the presence of water (Fig. 5 (f)). These two tests generate fractures with significantly higher conductivity values than the rest of the tests, and another two of the CO_2/PAA tests generate similar fractures compared with CO_2/H_2O. These results, together with the fact that high conductivity values are obtained independently of injection rates, show that PAA/CO_2 represents an excellent stimulation fluid alternative for EGS.

3.7 Flow rate into fracture during constant flow rate fracturing tests

The transient flow rate into the fracture(de Pater et al. 1994) can be calculated using Eq. (3).

$$Q_{frac} = Q_{pump} - 1/C * dp/dt \quad (3)$$

Where Q_{frac} is the flow rate into fracture; Q_{pump} is the flow rate delivered from the pump; C is the compressibility of the overall fracturing fluid system; dp/dt is the derivative of pressure with respect to time.

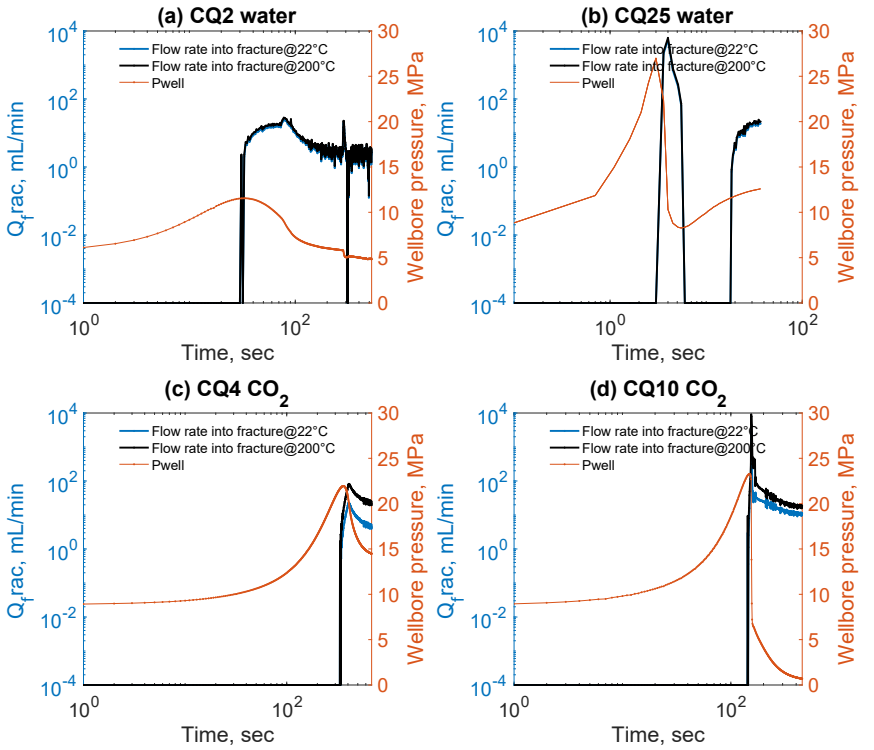

Fig. 6. Fracturing test with (a) H_2O, Q=2 mL/min in HDR B3; (b) H_2O, Q=25 mL/min in HDR B8; (c) CO_2, Q=4 mL/min in HDR B10; (d) CO_2, Q=10 mL/min in HDR B2; all tests were conducted at 200°C. **Zero or negative flow rate to fracture is set to 10^{-4} mL/min, which allows plots with log-log scale.

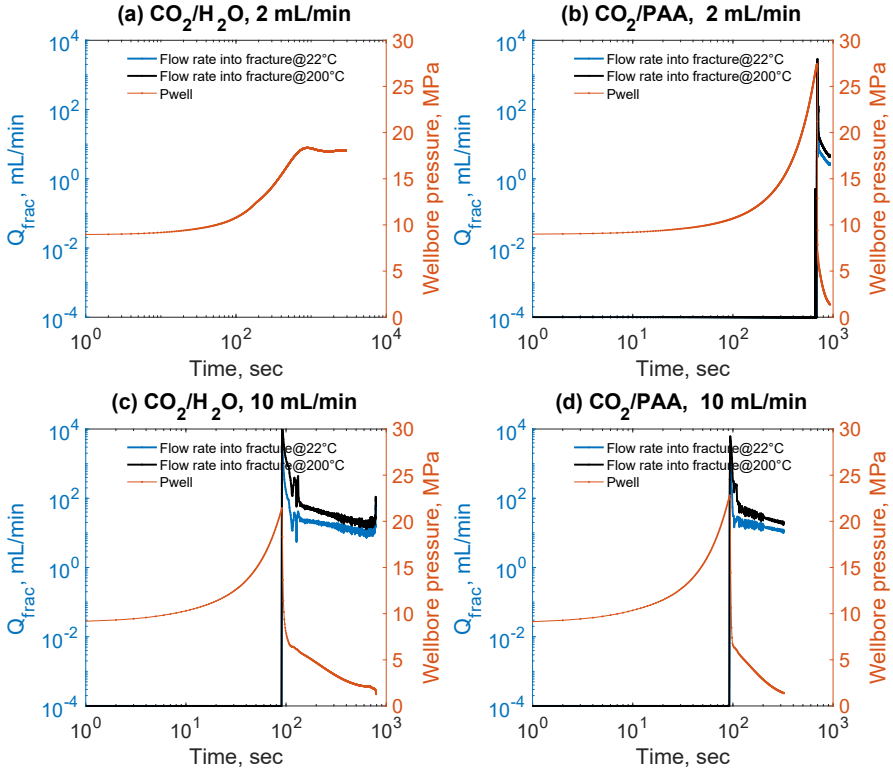

Fig. 7 Fracturing with (a) CO_2/H_2O, Q=2 mL/min in rock B1; (b) CO_2/PAA, Q=2mL/min in rock A10 ; (c) CO_2/H_2O, Q=2 mL/min in rock B1; (d) CO_2/PAA, Q=10 mL/min in rock B7; all tests were conducted at 200°C. **Zero or negative flow rate to fracture is set to 10^{-4} mL/min, which allows plots with a log-log scale.

The results of flow into the fracture for different stimulation tests are shown in Fig. 6 and Fig. 7 for water injected in HDR, CO_2 injected in HDR, CO_2/H_2O (CO_2 injected in rock partially saturated with water), and CO_2/PAA (CO_2 injected in rock partially saturated with aqueous PAA). For all fracturing tests involving CO_2 injection (with exception of CO_2 injected in HDR at 4 mL/min and CO_2 injected at 2 mL/min in rock partially saturated with water (CO_2/H_2O)), the maximum transient flow rate is in the range of 0.5×10^4~1×10^4 mL/min. For the two exceptions the flow into the fracture is only ~10^2 mL/min for CO_2 injected in HDR at 4 mL/min and 0 mL/min (i.e., no fracture created) for CO_2 injected at 2 mL/min in rock partially saturated with water (CO_2/H_2O, 2 mL/min). The last two cases can be interpreted as leak off-dominated fracturing processes taking place at lower, more stable, propagation rates. The conductivity of the fracture obtained by fracturing with CO_2 injected in HDR at 4 mL/min was also the lowest, 0.7~1.5 μm^3, among all the stimulation tests using CO_2. While for other constant flow rate fracturing injection strategies that use CO_2, either in HDR (stimulation strategy 2) or in a binary fluid system (CO_2/H_2O at 10 mL/min and CO_2/PAA) the conductivity values are all above 10 μm^3. High conductivity fractures are hypothesized to be a result of high transient fluid rates into the fracture rather than due to the fluid properties. In other words, slow leak-off dominated fracturing processes seem to create less conductive fractures than those obtained by faster fracturing processes.

To verify this hypothesis, i.e., whether the high transient fluid rate can generate fractures with high conductivity independently of the stimulation fluid used (water- or CO_2-based), a fracturing test injecting water in HDR with the highest flow rate the pump can achieve (25 mL/min) was conducted. Fig. 6(a) shows the fracturing results injecting water at 2 mL/min in HDR where the conductivity of the fracture was around 0.8-1.7 μm^3 and the maximum transient flow rate into the fracture was in the range of 10-10^2 mL/min. Conversely, for the stimulation test where water is injected at 25 mL/min in HDR [Fig. 6 (b)], the maximum transient flow rate into the fracture was similar (~104 mL/min) to those calculated for most of the CO_2-based (single fluid or binary fluids) fracturing tests. However, the conductivity of the fracture for water injected at 25 mL/min in HDR was only 1.0~2.1 μm^3. This indicates that a high transient flow rate into the fracture is not the only element playing a role in fracture conductivity. The properties of the fluid also play a key role in fracture creation and propagation.

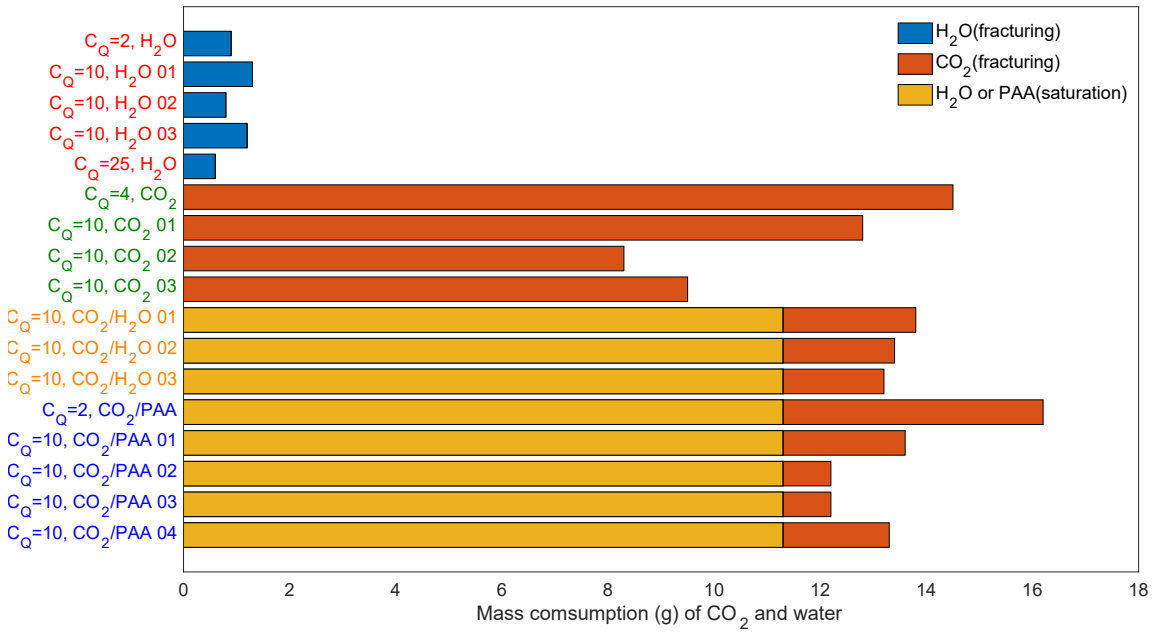

Fig. 8 Mass consumption of CO_2 and water for each fracturing test

Fluid mass consumption during stimulation operations is an important factor at the time of selecting a fluid for EGS stimulation. The mass of fluid injected in each test was calculated from the time the fluid is injected at constant flow rate to the time when the breakdown pressure is reached. For water, the calculation is straightforward for calculation since density changes with temperature under the experimental conditions is negligible. However, for the CO_2-based fluids, the density of CO_2 changes significantly with temperature. The key lays then in estimating the temperature of CO_2 when its pressure reaches breakdown pressure during the stimulation process. Under the experimental conditions, CO_2 undergoes a process that is neither an adiabatic process nor isothermal process. If an adiabatic process is assumed, the temperature of CO_2 could be estimated by Equation of State for gases. Therefore, for constant flow rate injection mode, a range of mass of injected CO_2 is reported in Table 1 where the lower mass value is estimated assuming an isothermal process and the upper mass value is estimated by assuming an adiabatic process. Fig. 8 shows that for different fracturing tests, CO_2 injected in rock partially saturated with aqueous PAA (CO_2/PAA) uses significantly lower CO_2 than CO_2 injection in HDR.

3.8 Simulation of fluid transport with different fracturing fluids

Within the field of fracture mechanics, fracture initiation is the process of extending pre-existing fractures. These fractures may exist naturally in the rock (e.g., grain boundaries) or be induced by field operations such as drilling. A fracture mechanics treatment of initiation

begins with the assumption of the existence of an initial crack of length L_o. For example, a crack of length a on the edge of a plate, perpendicular to the loading direction of the plate, will begin to propagate when the tensile stress in the plate reaches:

$$\sigma_c = \frac{K_{Ic}}{\sqrt{\pi a}} \tag{4}$$

Where K_{Ic} is the critical stress intensity factor, or fracture toughness. Generally, the size, shape, location, and orientation of initial cracks are not known and instead can be inferred from test data or assumed to be randomly oriented and just below the detection limit. Under this mode of analysis, the larger the volume of material that experiences tensile stress, the higher the probability of a pre-existing crack with size and orientation that will propagate. This leads to the well-known size effect observed in brittle materials, wherein smaller samples are, on average, stronger than larger samples. For a poroelastic problem where elevated pore fluid pressure is responsible for generating the failure stress, things are more complicated. A hydraulic fracture opens when the fluid pressure within the fracture exceeds the total stress in acting at the fracture walls. The total stress is defined as:

$$\sigma = \sigma' + \alpha P_p \tag{5}$$

Where σ' is the Biot effective stress, α is the Biot coefficient, and P_p is the pore fluid pressure. Since the fluid pressure within a fracture acts against the total stress in the adjacent formation, if the pore fluid pressure within the adjacent rock increases, the fracturing pressure will increase to maintain the fracture aperture (constant flow conditions). The pore fluid pressure surrounding a fracture can increase through two primary mechanisms. First, if a fracture rapidly opens, the surrounding rock will experience a rapid increase in compressive stress, which can induce pore pressure change. This instantaneous response of the rock is often referred to as the undrained response, and the resulting pressure is often referred to as the poroelastic pressure. The poroelastic pressure will dissipate over a time scale proportional to the permeability of the rock. For most hydraulic fracturing applications this poroelastic effect is small and decreases rapidly over time. The other primary mechanism by which fluid pressure can increase adjacent to a hydraulic fracture is by fluid diffusing from the fracture, often called leakoff. The effect this has on the fracture is to essentially act like an increased normal compressive stress, often called "back stress" (Cleary 1980; Detournay and Cheng 1991). The back stress is equal to

$$\sigma_B = \frac{\alpha(1-2\nu)}{2(1-\nu)}\Delta P = \eta \Delta P \tag{6}$$

Where ν is the drained Poisson's ratio and ΔP is the increase in pore pressure, and η is called the poroelastic parameter, which varies from 0 to 0.5 (if the Biot coefficient were 1 and the Poisson's ratio were zero).

(Lu et al. 2020) conducted a series of true triaxial fracture experiments to investigate the time-dependence of breakdown under constant wellbore pressure conditions. They found that the time-dependence of the breakdown was explainable by two mechanisms: fluid diffusion and subcritical fracture growth. The fluid diffusion effect was evident by the longer time required for breakdown with a viscous fluid (glycerine) compared to water. Two classical breakdown criteria have been used extensively for the formation of longitudinal fractures: The Hubert-Willis (H-W) expression:

$$P_b = 3\sigma_h - \sigma_H + T - P_p \tag{7}$$

And the Haimson-Fairhurst (H-F) criterion:

$$P_b = \frac{3\sigma_h - \sigma_H + T - 2\eta P_p}{2(1-\eta)} \tag{8}$$

(Detournay and Carbonell 1997) have shown that the two criteria can be united into one in the context of poroelasticity, with the H-W criterion being used for rapid pressurizations and low permeability formations, and the H-F criterion being used for slow pressurizations and high permeability formations. All else being equal, the case of slower pressurization and higher permeability is expected to lead to lower breakdown pressures, which is consistent with the results in (Song et al. 2019; Lu et al. 2020). Note that the experimental result shown below are not for longitudinal fractures, and hence these two criteria are not directly applicable, but the same general trends would be expected since the underlying physics are how stress changes with pore pressure diffusion and are not specific to the wellbore geometry. For this sake, a simulation model was built to get the pressure distribution within the rock before rock break-down. The details of the rock model are shown in Fig. 9.

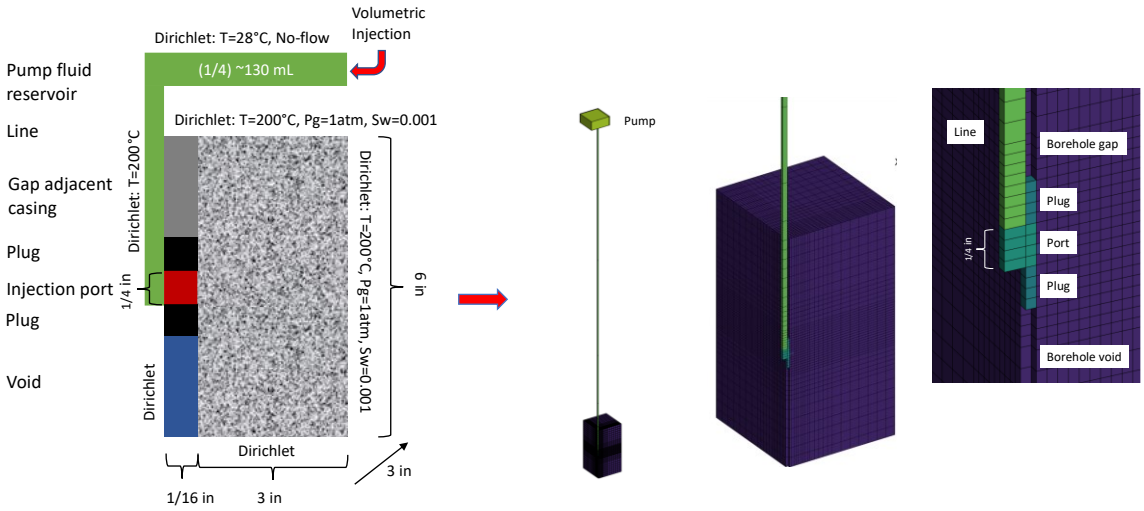

Fig. 9 Model rock system for simulations

The four injection strategies in constant flow rate mode (Q=10 mL/min) were simulated and the pressure from the wellbore to the rock surface is plotted as shown in Fig. 10. The breakdown pressure and pressurization length for four fluids are summarized in Table 3. For H2O fracturing in HDR, the average breakdown pressure is approximately 24.1 MPa, for an average net breakdown pressure (difference between the minimum principal stress value in the vertical direction and the breakdown pressure observed) of approximately 16.5MPa. The zone where the pore pressure exceeds the minimum principal stress is 0.66 cm. Fracture propagation appears to have been very slow and probably leak off dominated. The estimated fracture conductivity is of 1.7~2.1 μm^3, 2.5~3.3 μm^3, 2.5~3.3 μm^3. For CO_2 fracturing in HDR, CO_2 was allowed to leak off at approximately 9 MPa for approximately 240 seconds, after which CO_2 was injected at 10 mL/min. No water was ever injected into the sample. Average breakdown pressure is approximately 24 MPa, for a net breakdown pressure of approximately 16.4 MPa. Fracture propagation appears to be very rapid and dynamic. The zone where the pore pressure exceeds the minimum principal stress is approximately 1.27 cm at the breakdown (Fig. 10). We did three tests under these conditions, with estimated fracture conductivity values of 160~340 μm^3, 10~23 μm^3, and 2~4 μm^3.

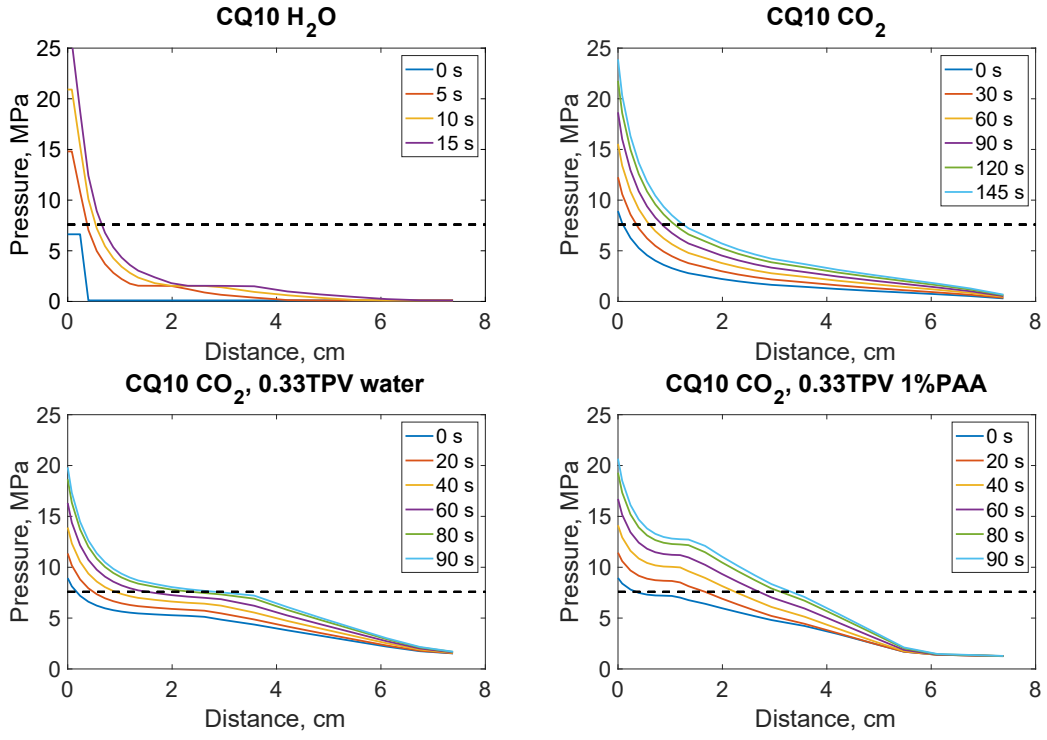

Fig. 10 Simulated pressure distribution curve from injection port to the rock surface

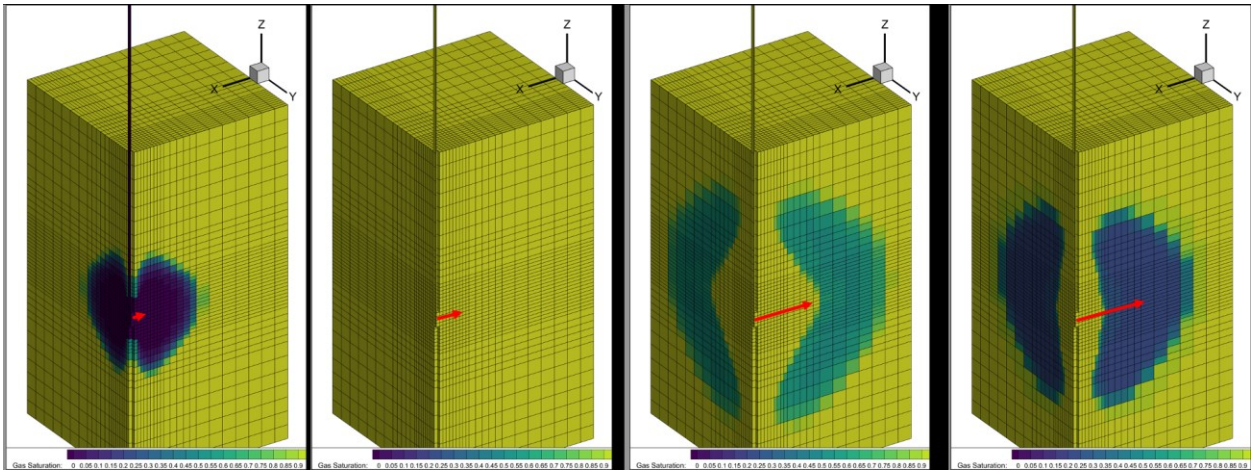

Fig. 11 Saturation envelope within the rock at breakdown time (CQ=10mL/min), red arrows show the simulated pressurize length above minimum principle stress at time of rock breakdown

For fracturing experiments where CO_2 is injected in rock partially saturated with water (CO_2/H_2O), water was injected at 6.9~8.8 MPa for 1190 seconds (11 mL, or approximately 33% of the estimated pore volume), then allowed CO_2 to leak-off at 9 MPa for approximately 360 seconds. CO_2 was then injected at 10 mL/min. Average breakdown pressure is approximately 20.7 MPa, for an average net breakdown pressure of approximately 13.1 MPa. Fracture propagation appears to be very rapid and dynamic. The zone where the pore pressure exceeds the minimum principal stress is approximately 2.79 cm at the breakdown. The estimated fracture conductivity of 19.7~41.8 μm^3, 24.4~51.9 μm^3, 8.2~17.5 μm^3. For fracturing experiments where CO_2 is injected in rock partially saturated with aqueous PAA (PAA/H_2O), a 1wt% PAA aqueous solution was first injected at approximately 6.9~8.8 MPa for approximately 1190 seconds (11 mL or approximately 33% of the pore volume), then allowed CO_2 to leak-off at 9 MPa for approximately 360 seconds and then allowed CO2 to leak-off at 9 MPa for approximately 360 seconds and after which CO_2 was injected at 10 mL/min. To account for the viscosity increase associated to the crosslinking reaction between PAA and CO_2, in the numerical simulations the PAA aqueous solution was simulated as pure water but with a viscosity 100 times higher than water. Breakdown pressure is averaged 23.9 MPa, for an average net breakdown pressure of 16.3 MPa. Fracture propagation appears to be very rapid and dynamic. The zone where the pore pressure exceeds the minimum principal stress is approximately 3.30 cm at the moment of rock breakdown (Fig. 10). The estimated fracture conductivity is 65.7~139.5 μm^3, 44.7~95 $\mu m3$, 77.7~165.1 μm^3, 12.5~26.5 μm^3.

The simulations results shown in Fig. 10 also show that when the formation is pre-saturated with CO_2-reacted PAA, the region of elevated pore pressure caused by subsequent CO_2 injection is more spatially concentrated compared to cases with only water pre-saturation. This appears to be the result of the elevated viscosity of the cross-linked CO_2-PAA, which reduces diffusion of pore pressure resulting in a broader region with elevated pore pressure. This may be responsible for the elevated fracture conductivity observed with this fluid, since a broader pressurized region would have the opportunity to generate a more complex fracture that retains more conductivity when closed.

Another effect that is known to influence breakdown is the wellbore compressibility (Lecampion et al. 2017). Larger wellbore compressibility is known to cause larger breakdown pressures. If this mechanism were responsible for the elevated breakdown pressure in the CO_2 tests, this would imply that the fracture was initiated at a pressure comparable to the water tests, but that breakdown did not occur because the flow rate into the initiated fracture was significantly smaller than our injection rate. Therefore, as we continued pumping the pressure continued to rise until the combination of higher pressures and time cause the fracture to grow. The fracture will continue to grow until it could accommodate all the injected flow rate-which is the definition of breakdown. However, from previous breakdown pressure statistical analysis reported in Table 2, CO_2 and water don't show a significant difference for breakdown pressure at 95% confidence level. Furthermore, the breakdown pressure in all of our constant injection rate fracturing tests are close, and higher breakdown pressures can be, in general, achieved with higher flow rate injection during pumping.

Table 3 Correlation between breakdown pressure and simulated pressurized length

	Average experimental Pb (MPa)	95% confidence interval of Pb (MPa)	Simulation Pb (MPa)	Simulation pressurized length (cm)
H_2O	23.9	[16.5, 34.6]	26.0	0.66
CO_2	24.0	[21.8, 26.5]	24.4	1.24
CO_2/H_2O	20.6	[16.8, 25.4]	20.2	2.79
CO_2/PAA	22.3	[21.3, 23.5]	21.5	3.30

3.9 Post fracture analysis of rock thin sections

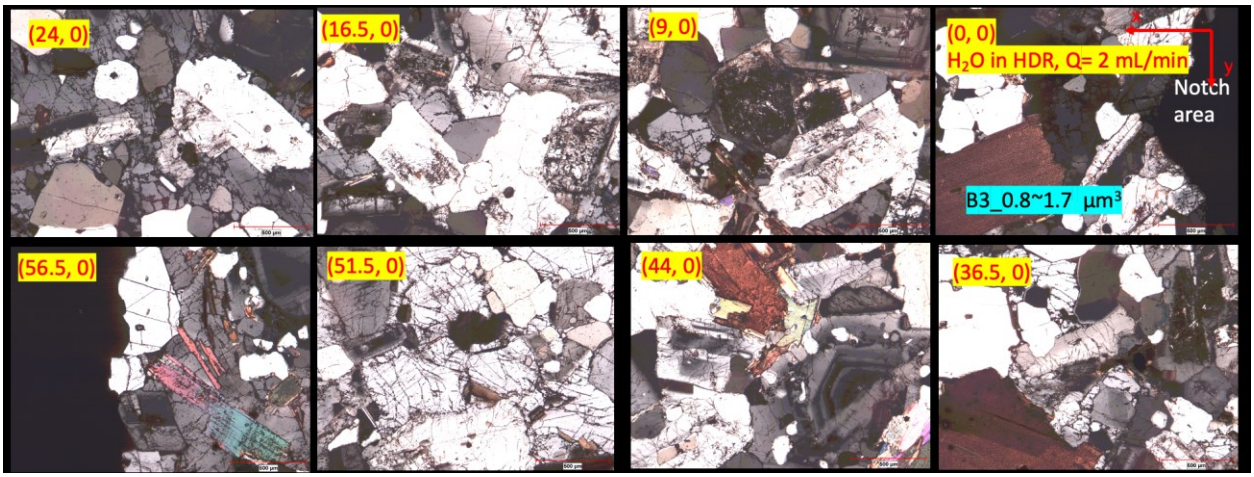

(a)

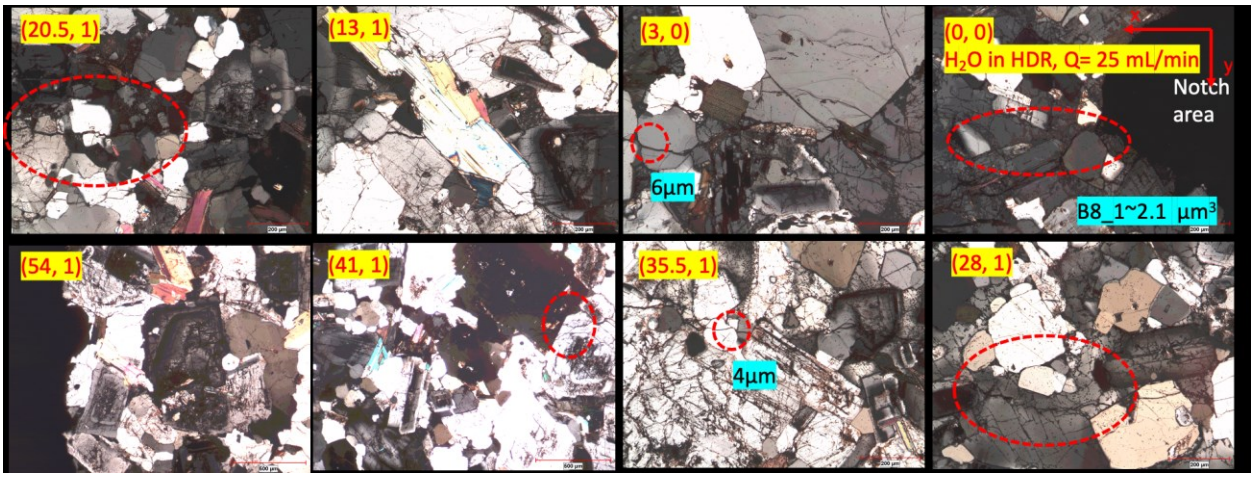

(b)

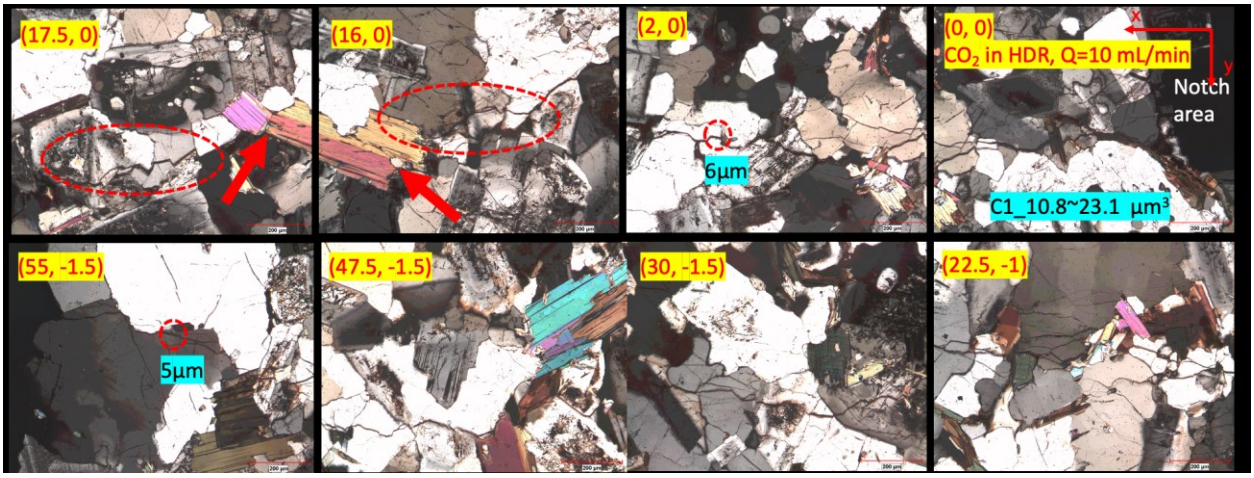

(c)

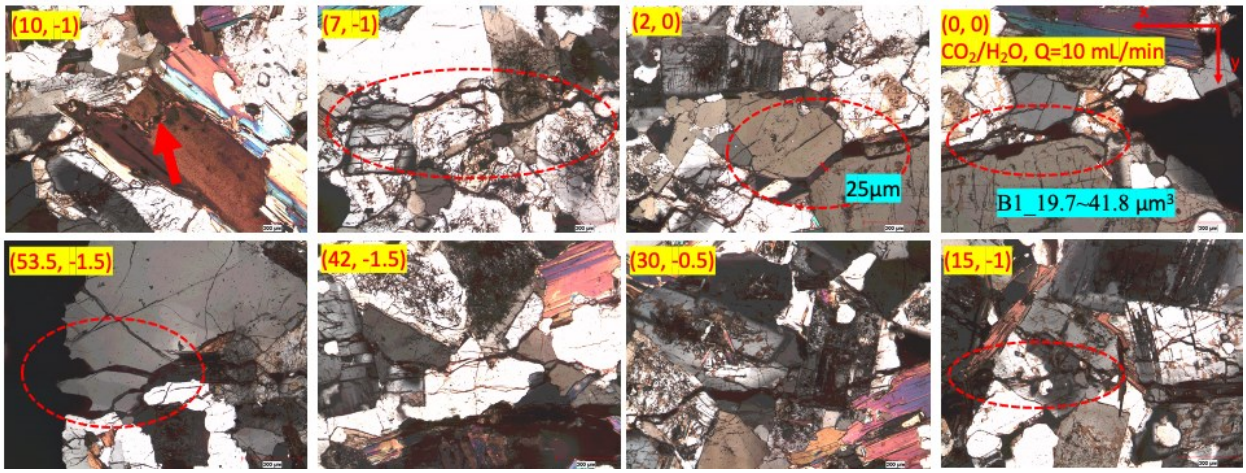

(d)

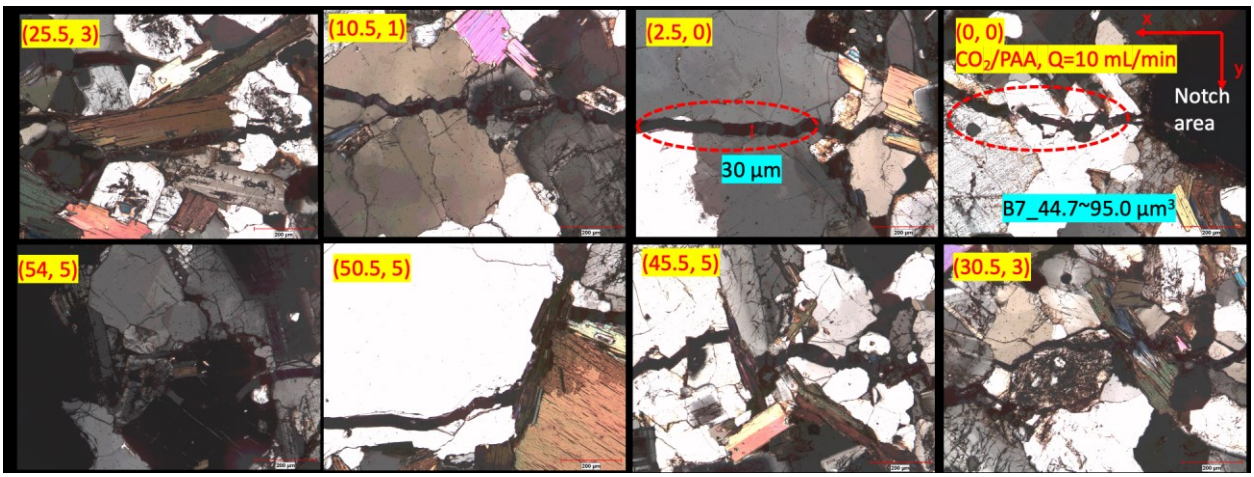

(e)

Fig. 12 Thin section analysis for different fracturing fluids(a) H_2O, Q=2 mL/min; (b) H_2O in HDR, Q=25 mL/min; (c) CO_2 in HDR, Q=10 mL/min; (d) CO_2/H_2O, Q=10mL/min; (e) CO_2/PAA, Q=10mL/min. Color code by stains of thin section: K-Feldspar Stain(yellow); Plagioclase Stain(orange red); Calcite Stain(pink red); Iron Stain(blue); Others(quartz): white or grey or else.

Fig. 12 shows optical micrographs of thin sections analysis of four different fluids (including two rock samples fractured with water injected in HDR at low and high injection rates). The first picture in the top right of each group of eight micrographs [Fig. 12(a) to (e)] is the one that includes the notch. The coordinate for the picture with notch (origin of the fracture) is denoted as (0,0). From the origin (notch), x, y coordinates change with the "x" direction (axis) corresponding to the fracture propagation direction, and the "y" axis corresponding to the direction of minimum principal stress. The distance unit is mm. It was noticed that fracture propagation seems to have a difficult time to occur through plagioclase grains (orange color and tabular) thus bypassing the plagioclase grains or just disappearing at the edge of the grains. In some cases, particularly with the narrower aperture fractures, the fracture seems to disappear at the plagioclase grains. There is evidence for such small unfractured ligaments(Labuz, Shah, and Dowding 1987; Ghamgosar and Erarslan 2016) can exist and connect two halves of a fracture. For example, for the micrograph labeled (10, -1) in the CO_2/H_2O (Q=10mL/min) case, the fracture passes through/around the plagioclase grain and is then filled with a white precipitate within the plagioclase grain (see arrows inside orange red circumference). Similarly, the (17.5,0) and (16,0) micrographs for CO_2 in HDR (Q=10 mL/min) show how the fracture disappears at a K-feldspar and plagioclase grain (see arrows inside yellow and orange red circumference). Another explanation for the latter case, could be that the fracture grows around the grains. What it is certain is that the fracture's aperture is reduced at/around these grains. In contrast, micrographs taken on thin sections of rock fractured with CO_2/PAA (Q=10mL/min) show a completely different landscape. Micrograph (2.5,0) [Fig. 12(e)], for example, shows on the right-hand side a plagioclase grain where the fracture cuts through the grain and also makes a parallel path around it. What we speculate occurred is that when the fracture tip first propagates it goes around the tougher material because it lacks the energy/aperture to cross through it. Then, after the fracture extends more its aperture increases and new fractures grow in a more straight-line path through the tougher (plagioclase grain) material. A similar example could be the case of micrograph (30.5, 3) for CO_2/PAA (Q=10mL/min), though the color of the grain in question is blue-purple with only hints of orange (maybe Biotite). (Jeong et al. 2017) also reported fractures growing in straight lines through quartz grains but only following cleavage planes in plagioclase and K-felspars. This could be largely associated to a viscosity effect. Higher viscosity fluids tend to produce larger

fracture apertures. Larger fracture apertures will tend to force more tough or ductile features to separate that could remain attached in a fracture with a smaller aperture. From this analysis it can be clearly concluded that CO_2/PAA fluid system attain fractures with the largest, self-propped, apertures in agreement with the consistently high fracture conductivity values measured post-stimulation and independently of injection flow rate.

4. SUMMARY

Four stimulation fluids/strategies; water, CO_2, CO_2/water, CO_2/PAA, were evaluated in ½-foot side cubic granite samples at 200 °C and under geothermal relevant stress conditions using a high-temperature true-triaxial system.

Results show that for the injection strategy consisting in injecting water in HDR, the conductivity is generally less than 2 μm^3 (radial flow) even when injecting at very high flow rates (25 mL/min). For CO_2-based stimulation fluids, i.e., CO_2 in HDR, CO_2/H_2O, and CO_2/PAA, the fracture conductivity is larger than that of water. These findings are consistent with other results published in the literature, for both shale and granite at room temperature(Song et al. 2019). The breakdown pressure was higher for tests with all stimulation strategies that used CO_2, as compared to fracturing with water. The discrepancy between these results and those in the literature (Ishida et al. 2012; Song et al. 2019)is not yet understood, but it may be caused by the difference in experimental temperature (room temperature vs. 200 °C) and rock type (shale vs. granite).

The pressurization rate affects fracturing with water insignificantly but for CO_2-based fluids is a key factor for generating fractures with high conductivity. Rapid pressurization rate (>6.89 MPa/min (1000 psi/min)) of CO_2-based fluids is beneficial for generating fractures with higher conductivity (>10 μm^3). However, when the pressurization rate of CO_2 is lower than 0.69MPa/min (100 psi/min), the hydraulic conductivity of the fracture (1~10 μm^3) is only slightly higher than that of fractures generated by water injection (<1μm^3). This is also in disagreement with other results(Song et al. 2019), which attributed the enhanced conductivity of CO_2-generated fractures to the additional volume of rock stimulated due to the higher leak-off volume associated to CO_2 as compared to water. In our study, the higher injection rates, which would produce less leak off overall, resulted in more conductive fractures.

Injection of water or aqueous PAA to partially saturate the rock previous to CO_2 injection (stimulation strategies CO_2/H_2O and CO_2/PAA) is beneficial to reduce the leak-off rate of CO_2 fracturing test and, in this fashion, aid to pressure build up. The leak-off rate of CO2 can be significantly reduced using PAA as observed in the constant flow rate fracturing process, and this can be explained by the fact that the CO_2-triggered crosslinking reaction of PAA and associated volume expansion can cause an in-situ increase in both aqueous phase saturation and viscosity, thus decreasing the relative permeability of the CO_2 phase in the porous matrix. As a result, CO_2 can build up pressure faster and create larger fractures as compared to CO_2/H_2O stimulation fluid and with a significantly lower injected mass. Furthermore, CO_2 not only builds up pressure faster but also transfer this stress to the high viscosity PAA (rather than displacing the fluid front like in the case of water or air, see Fig. 10) building a larger pressure envelope with pressure values above the minimum principal stress.

It was also observed that the transient flow rate of fracturing fluids especially for the CO_2-based stimulation fluids (CO_2 in HDR, CO_2/H_2O, and CO_2/PAA) can affect the ultimate conductivity of the created fracture. For CO_2-based stimulation processes, fractures with large conductivity can be formed if the transient flow rate to fracture is in the order of 104 mL/min.

CO_2/PAA fracturing fluid system was found to generate fractures with the highest conductivity values and independently of injection flow rate. Breakdown pressures were also similar for CO_2 stimulation in HDR and CO_2/PAA fluid system under identical injection flow rates. It is concluded that CO_2/PAA fluid system is the fracturing fluid of choice for stimulation of granitic rock samples under the studied geothermal P/T conditions. CO_2/PAA, however, offer the following three additional advantages; 1) it requires a significantly lower (1/6) mass of CO_2 (0-2.3g vs 4-12.8 g) (note: a corresponding mass of PAA equivalent to 0.11g or 5% of that of CO_2 is also required), 2) the fracture conductivity is independent of injection flow rate, and 3) the reversible viscosity(B. Jung et al. 2015) increase is beneficial to transport proppants when they become available for enhanced geothermal systems. The microscopy images of rock thin sections also show significantly higher dominant (self-propped) fracture apertures when using CO_2/PAA fluid system than the other fluid systems.

5. NOMENCLATURE

μ	Viscosity of fluids
k_{rock}	Permeability of rock
∇P	Pressure gradient across the rock
k_{rg}	Relative permeability of gas
k_{rg}^0	End point relative permeability of gas
S_w	Water saturation
S_g	Gas saturation
S_{wc}	Connate water saturation
S_{grw}	Residual gas saturation to water
n_g	Exponent coefficient of gas in Corey's model
Q_{frac}	The flow rate into fracture
Q_{pump}	Flow rate delivered from the pump

C Compressibility of the overall fracturing fluid system

dp/dt Derivative of pressure to time.

REFERENCES

Bee, A., R. Massart, and S. Neveu. 1995. "Synthesis of Very Fine Maghemite Particles." *Journal of Magnetism and Magnetic Materials* 149 (1–2): 6–9. https://doi.org/10.1016/0304-8853(95)00317-7.

B. Jung, H., K. C. Carroll, S. Kabilan, D. J. Heldebrant, D. Hoyt, L. Zhong, T. Varga, et al. 2015. "Stimuli-Responsive/Rheoreversible Hydraulic Fracturing Fluids as a Greener Alternative to Support Geothermal and Fossil Energy Production." *Green Chemistry* 17 (5): 2799–2812. https://doi.org/10.1039/C4GC01917B.

Bradford, Jacob, Mary Ohren, William L. Osborn, John McLennan, Joseph Moore, and Robert Podgorney. 2014. "Thermal Stimulation and Injectivity Testing at Raft River, ID EGS Site." In *Proceedings of 39th Workshop on Geothermal Reservoir Engineering, Stanford, CA, USA*.

Chabora, Ethan, Ezra Zemach, Paul Spielman, Peter Drakos, Stephen Hickman, Susan Lutz, Katie Boyle, Amber Falconer, Ann Robertson-Tait, and Nicholas C. Davatzes. 2012. "Hydraulic Stimulation of Well 27-15, Desert Peak Geothermal Field, Nevada, USA." In *Proceedings of Thirty-Seventh Workshop on Geothermal Reservoir Engineering, Stanford University, Stanford*. Vol. 30.

Cleary, Michael P. 1980. "Comprehensive Design Formulae For Hydraulic Fracturing." In . Society of Petroleum Engineers. https://doi.org/10.2118/9259-MS.

Detournay, Emmanuel, and Roberto Carbonell. 1997. "Fracture-Mechanics Analysis of the Breakdown Process in Minifracture or Leakoff Test." *SPE Production & Facilities* 12 (03): 195–99.

Detournay, Emmanuel, and Alexander H. -D. Cheng. 1991. "Plane Strain Analysis of a Stationary Hydraulic Fracture in a Poroelastic Medium." *International Journal of Solids and Structures* 27 (13): 1645–62. https://doi.org/10.1016/0020-7683(91)90067-P.

Fernandez, Carlos A., Varun Gupta, Gao L. Dai, Andrew P. Kuprat, Alain Bonneville, Delphine Appriou, Jake A. Horner, Paul F. Martin, and Jeffrey A. Burghardt. 2019. "Insights into a Greener Stimuli-Responsive Fracturing Fluid for Geothermal Energy Recovery." *ACS Sustainable Chemistry & Engineering* 7 (24): 19660–68. https://doi.org/10.1021/acssuschemeng.9b04802.

Ghamgosar, M., and N. Erarslan. 2016. "Experimental and Numerical Studies on Development of Fracture Process Zone (FPZ) in Rocks under Cyclic and Static Loadings." *Rock Mechanics and Rock Engineering* 49 (3): 893–908. https://doi.org/10.1007/s00603-015-0793-z.

Heath, D. F. 1967. "Normal or Log-Normal: Appropriate Distributions." *Nature* 213 (5081): 1159–60. https://doi.org/10.1038/2131159a0.

Isaka, B. L. Avanthi, P. G. Ranjith, T. D. Rathnaweera, W. A. M. Wanniarachchi, W. G. P. Kumari, and A. Haque. 2019. "Testing the Frackability of Granite Using Supercritical Carbon Dioxide: Insights into Geothermal Energy Systems." *Journal of CO2 Utilization* 34 (December): 180–97. https://doi.org/10.1016/j.jcou.2019.06.009.

Ishida, Tsuyoshi, Kazuhei Aoyagi, Tomoya Niwa, Youqing Chen, Sumihiko Murata, Qu Chen, and Yoshiki Nakayama. 2012. "Acoustic Emission Monitoring of Hydraulic Fracturing Laboratory Experiment with Supercritical and Liquid CO2." *Geophysical Research Letters* 39 (16). https://doi.org/10.1029/2012GL052788.

Jeong, S. S., K. Nakamura, S. Yoshioka, Y. Obara, and M. Kataoka. 2017. "Fracture Toughness of Granite Measured Using Micro to Macro Scale Specimens." *Procedia Engineering*, ISRM European Rock Mechanics Symposium EUROCK 2017, 191 (January): 761–67. https://doi.org/10.1016/j.proeng.2017.05.242.

Jian, Guoqing, Carlos A. Fernandez, Jeff Burghardt, Alain Bonneville, Varun Gupta, and Geoffrey Garrison. 2020. "Alternative, Less Water-Intensive, Fracturing Fluids for Enhanced Geothermal Systems." In . American Rock Mechanics Association. https://www.onepetro.org/conference-paper/ARMA-2020-1369.

Jian, Guoqing, Leilei Zhang, Chang Da, Maura Puerto, Keith P. Johnston, Sibani L. Biswal, and George J. Hirasaki. 2019. "Evaluating the Transport Behavior of CO2 Foam in the Presence of Crude Oil under High-Temperature and High-Salinity Conditions for Carbonate Reservoirs." *Energy & Fuels* 33 (7): 6038–47. https://doi.org/10.1021/acs.energyfuels.9b00667.

Labuz, J. F., S. P. Shah, and C. H. Dowding. 1987. "The Fracture Process Zone in Granite: Evidence and Effect." *International Journal of Rock Mechanics and Mining Sciences & Geomechanics Abstracts* 24 (4): 235–46. https://doi.org/10.1016/0148-9062(87)90178-1.

Lecampion, B., J. Desroches, R. G. Jeffrey, and A. P. Bunger. 2017. "Experiments versus Theory for the Initiation and Propagation of Radial Hydraulic Fractures in Low-Permeability Materials." *Journal of Geophysical Research: Solid Earth* 122 (2): 1239–63. https://doi.org/10.1002/2016JB013183.

Lu, Guanyi, Elizaveta Gordeliy, Romain Prioul, Gallyam Aidagulov, Efosa C. Uwaifo, Qihang Ou, and Andrew P. Bunger. 2020. "Time-Dependent Hydraulic Fracture Initiation." *Journal of Geophysical Research: Solid Earth* 125 (3): e2019JB018797. https://doi.org/10.1029/2019JB018797.

Lund, John W. 2011. "Direct Utilization of Geothermal Energy 2010 Worldwide Review." *Geothermics* 40 (3): 159–80.

Lund, John W., and Tonya L. Boyd. 2016. "Direct Utilization of Geothermal Energy 2015 Worldwide Review." *Geothermics* 60 (March): 66–93. https://doi.org/10.1016/j.geothermics.2015.11.004.

Lund, John W, and Derek H Freeston. 2001. "World-Wide Direct Uses of Geothermal Energy 2000." *Geothermics* 30 (1): 29–68. https://doi.org/10.1016/S0375-6505(00)00044-4.

Lund, John W., Derek H. Freeston, and Tonya L. Boyd. 2005. "Direct Application of Geothermal Energy: 2005 Worldwide Review." *Geothermics* 34 (6): 691–727. https://doi.org/10.1016/j.geothermics.2005.09.003.

Pater, C. J. de, M. P. Cleary, T. S. Quinn, D. T. Barr, D. E. Johnson, and Leen Weijers. 1994. “Experimental Verification of Dimensional Analysis for Hydraulic Fracturing.” *SPE Production & Facilities* 9 (04): 230–38. https://doi.org/10.2118/24994-PA.

Shao, Hongbo, Senthil Kabilan, Sean Stephens, Niraj Suresh, Anthon N. Beck, Tamas Varga, Paul F. Martin, et al. 2015. “Environmentally Friendly, Rheoreversible, Hydraulic-Fracturing Fluids for Enhanced Geothermal Systems.” *Geothermics* 58 (November): 22–31. https://doi.org/10.1016/j.geothermics.2015.07.010.

Song, Xuehang, Yintong Guo, Jin Zhang, Nannan Sun, Guofei Shen, Xin Chang, Weisheng Yu, et al. 2019. “Fracturing with Carbon Dioxide: From Microscopic Mechanism to Reservoir Application.” *Joule* 3 (8): 1913–26. https://doi.org/10.1016/j.joule.2019.05.004.